Eur. Phys. J. D **32**, 233–239 (2005)
DOI: 10.1140/epjd/e2004-00171-6

THE EUROPEAN PHYSICAL JOURNAL D

A proposal to test Bell's inequalities with mesoscopic non-local states in cavity QED

P. Milman[1], A. Auffeves[1], F. Yamaguchi[2], M. Brune[1], J.M. Raimond[1,a], and S. Haroche[1,3]

[1] Laboratoire Kastler Brossel, Département de Physique de l'École Normale Supérieure, 24 rue Lhomond, 75231 Paris Cedex 05, France
[2] Edward L. Ginzton Laboratory, Stanford University, Stanford, CA 94305, USA
[3] Collège de France, 11 place Marcelin-Berthelot, 75005 Paris, France

Received 4 June 2004
Published online 30 November 2004 –

Abstract. We propose a cavity quantum electrodynamics (CQED) experiment to test the violation of a Bell-type inequality using non-local mesoscopic states (NLMS). These states involve coherent field superpositions stored in two spatially-separated high-Q cavities. The inequality is expressed in terms of the measured Wigner function of the entangled two-field-mode system at four points in phase space, as proposed in [Banaszek and Wódkiewicz, Phys. Rev. Lett. **82**, 2009 (1999)]. We examine the production of these entangled NLMS and the measurement of their Wigner function. The experiment involves circular Rydberg atoms and superconducting millimeter-wave cavities. We present a detailed numerical study of the optimal inequality violation and of the effect of decoherence. We discuss the range of experimental parameters making it possible to observe a locality violation and show that they correspond to realistic, albeit demanding, conditions.

PACS. 03.65.-w Quantum mechanics – 03.65.Ud Entanglement and quantum non-locality – 03.65.Yz Decoherence; open systems; quantum statistical methods – 42.50.Pq Cavity quantum electrodynamics; micromasers

1 Introduction

The development of quantum mechanics brought into light its contradictions with the 'classical' intuition. Multipartite superposition (entangled) states presenting non-local correlations fed a rich debate that remains alive, eighty years after the introduction of the quantum formalism. The interest for non-local entangled states ranges from fundamental tests of quantum mechanics to quantum information processing. Following on Einstein, Podolski and Rosen's discussion [1], Bell [2] showed that a combination of joint measurements performed on an entangled state leads to a clear-cut distinction between a classical, local, description of the physics and quantum mechanics. These measurement results satisfy, in all local theories, 'Bell inequalities' [2] violated by quantum mechanics. Bell-type inequalities have been formulated in many different contexts. The simplest one (CHSH inequality) involves a pair of spin-1/2 particles in a maximally entangled state [3].

Many experiments since Bell's theorem have vindicated quantum mechanics against local theories [4]. All of them were testing the CHSH entangled spin correlations. The Bell inequalities are not limited, however, to this simple situation. It would be particularly interesting to test them in situations involving non-local mesoscopic states (NLMS). Such states involve quantum correlations between two mesoscopic objects located at different places. They could thus be called non-local 'Schrödinger cat' states.

These mesoscopic superposition states are highly sensitive to the coupling with the environment. The resulting decoherence process [5] rapidly destroys the quantum superpositions, which evolve into statistical mixtures. The non-local properties of NLMS are thus expected to be washed out rapidly by the coupling with the environment. Experimental investigations of this original situation would shed new light both on quantum non-locality and on the decoherence process itself.

The non-local properties of NLMS and their possible application to quantum cryptography with continuous-variable systems [6], generalizing the spin-1/2 particles of the original protocol [7], have already been discussed in recent literature. Their general decoherence dynamics has also been investigated [8]. In the present work, we focus on the detailed discussion of a feasible cavity quantum electrodynamics (CQED) experiment, producing NLMS and testing the decoherence of their non-local features.

[a] e-mail: jmr@lkb.ens.fr

CQED provides fruitful experimental set-ups for tests of quantum mechanical properties of particles and fields [9]. In particular, the decoherence process of a superposition of mesoscopic microwave fields in a high Q superconducting cavity has been observed [10]. The cat states realized in this experiment, stored in a single cavity mode, did not involve non-locality. The experiment proposed here extends this situation to NLMS stored in two separate cavities.

The second section of this paper briefly introduces the two-mode NLMS to be used and recalls the Bell-type inequality, based on the joint Wigner function of the two modes. We then show (Sect. 3) how these states can be generated by a single circular Rydberg atom crossing the two cavities. We describe also the measurement of the joint Wigner function, using another Rydberg atom as a probe. In the last section (Sect. 4), we give the results of numerical simulations of this experiment. We study in details the decoherence properties of these non-local states and show that Bell's inequalities violations are expected for achievable, if demanding, experimental parameters.

2 Bell's inequalities and Wigner function

The standard CHSH Bell inequalities [3] cannot be used directly in the context of non-local two-mode states, the quantum system being described by continuous variables over a four-dimensional phase space. Discretization of the field observables, however, makes it possible to write simple Bell-type inequalities. We use here the one proposed by Banaszek and Wódkiewicz (BW) [11], later generalized by Jeong et al. [12]. Any local description of reality should lead to measurements satisfying the following inequality:

$$\mathcal{B} = |\Pi(\alpha', \beta') + \Pi(\alpha, \beta') + \Pi(\alpha', \beta) - \Pi(\alpha, \beta)| \leq 2, \quad (1)$$

where $\Pi(\alpha, \beta) = (\pi^2/4)W(\alpha, \beta)$ is a scaled version of the two-mode Wigner function $W(\alpha, \beta)$ [13] at the point in the four-dimensional phase space defined by the complex amplitudes α and β. The 'Bell signal', $\mathcal{B}$ results from the sampling of the scaled Wigner function at four points lying at the vertices of a rectangle. The maximum possible value for $\mathcal{B}$ in quantum mechanics, reached for well-chosen states and sampling points, is $2\sqrt{2}$, in contradiction with equation (1).

The BW version of Bell's inequalities is interesting in the CQED context. The Wigner function can then be directly measured, as proposed in [14], according to a scheme which has already been realized for a single cavity mode and zero and one-photon states [15]. In the two-mode case, the Wigner function measurement scheme is based on a simple relation between the scaled Wigner function $\Pi(\alpha_1, \alpha_2)$ and the field density matrix $\hat{\rho}$ [16]:

$$\Pi(\alpha_1, \alpha_2) = \mathrm{Tr}\left[\hat{\rho} \prod_{i=1}^{2} \hat{D}_i(\alpha_i) \hat{P}_i \hat{D}_i^{-1}(\alpha_i)\right], \quad (2)$$

where the index $i = 1, 2$ stands for the modes. The operator $\hat{D}_i(\alpha_i)$ is the displacement operator acting on the ith mode and $\hat{P}_i = e^{i\pi \hat{a}_i^\dagger \hat{a}_i}$ is the parity operator for mode i, with annihilation operator $\hat{a}_i$. Equation (2) shows that $\Pi(\alpha, \beta)$ is the average of the $\hat{P}_1\hat{P}_2$ operator, after a displacement by the amplitudes $-\alpha_1$ and $-\alpha_2$ in modes 1 and 2 respectively. The eigenstates of $\hat{P}_i$ are the Fock states $|n_i\rangle$, with the eigenvalues $(-1)^{n_i}$. The parity operators have thus only two possible measurement outcomes ($+1$ and -1). The scaled Wigner function is therefore bounded by ± 1:

$$-1 \leq \Pi(\alpha, \beta) \leq 1 \ . \quad (3)$$

The dichotomic parity observable can be directly compared to the spin 1/2 ones and is thus well-suited to derive the Bell-type inequality (1). A NLMS violating this inequality involves a correlation of the parities of the two cavity fields, generalizing the spin correlations in the maximally entangled state of the CHSH situation. Note that other adaptations of the CHSH inequalities to the continuous variable case lead to the selection of other dichotomic observables and to the use of other types of entangled states [17,18].

To be specific, we consider the maximally entangled Schrödinger cats states. We first define single-mode cat states as $|C_\pm\rangle = (|\gamma\rangle \pm |-\gamma\rangle)/N_\pm$, where $|\pm\gamma\rangle$ are coherent states of amplitude $\pm\gamma$ and $N_\pm$ are normalization constants. States $|C_+\rangle$ and $|C_-\rangle$ are eigenstates of the parity operator with eigenvalues $+1$ and -1 respectively. In the two-mode situation, we consider the four parity-entangled states:

$$\begin{aligned} |\Psi^\pm\rangle &= \frac{1}{N_{\Psi^\pm}} \left(|C_+, C_+\rangle \pm |C_-, C_-\rangle\right) \\ |\Phi^\pm\rangle &= \frac{1}{N_{\Phi^\pm}} \left(|C_+, C_-\rangle \pm |C_-, C_+\rangle\right), \end{aligned} \quad (4)$$

where the first and second symbols in the kets refer to the first and second mode respectively and $N_{\Psi^\pm}, N_{\Phi^\pm}$ are normalization factors.

Note that a simple rewriting of (4) leads to:

$$\begin{aligned} |\Psi^\pm\rangle &= \frac{1}{N_{\Psi^\pm}} \left(|\pm\gamma, \gamma\rangle + |\mp\gamma, -\gamma\rangle\right) \\ |\Phi^\pm\rangle &= \frac{1}{N_{\Phi^\pm}} \left(|\pm\gamma, -\gamma\rangle - |\mp\gamma, \gamma\rangle\right). \end{aligned} \quad (5)$$

This simpler expression is well suited for the description of the preparation procedure (next section).

States (4) become orthogonal in the limit $\gamma \to \infty$ and form then a Bell basis for the parity observable in the subspace of maximally entangled cat states. These four states describe situations where the parities of the cavity fields exhibit quantum correlation. For instance, in state $|\Psi^+\rangle$, both cavities contain fields with identical parities. Violations of the inequality (1) can be expected for carefully chosen sampling points in phase space.

We restrict our discussion here to the case of $|\Psi^+\rangle \propto (|\gamma, \gamma\rangle + |-\gamma, -\gamma\rangle)$. The generalization to the other three Bell states is straightforward. We can get an insight into the choice of the sampling points by considering the scaled

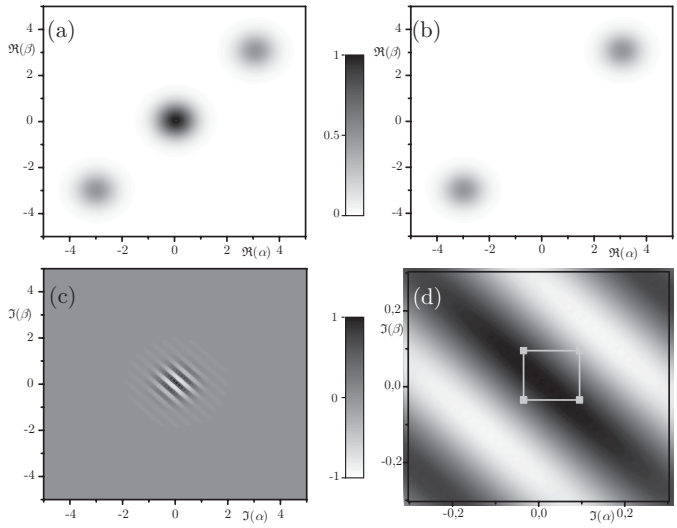

Fig. 1. Cuts in the scaled two-mode Wigner function $\Pi(\alpha, \beta)$. (a) NLMS state $|\Psi^+\rangle$ with $\gamma = 3$, in the plane $\Im(\alpha) = \Im(\beta) = 0$. The two Gaussian peaks at $\alpha = \beta = \pm\gamma$ (maximum value 0.5) correspond to the two components of the NLMS. The central feature (peaking at 1) reveals the quantum coherence of the state. (b) same plot for a statistical mixture of $|\gamma, \gamma\rangle$ and $|-\gamma, -\gamma\rangle$. Note the absence of the central feature. For (a) and (b), white corresponds to zero and black to one. (c) NLMS state $|\Psi^+\rangle$ with $\gamma = 3$, in the plane $\Re(\alpha) = \Re(\beta) = 0$. The coherence is revealed by the fringes near the origin. (d) Zoom on the central region of (c) with the four sampling points leading to a maximum violation of the Bell inequality. For plots (c) and (d), white corresponds to –1 and black to +1.

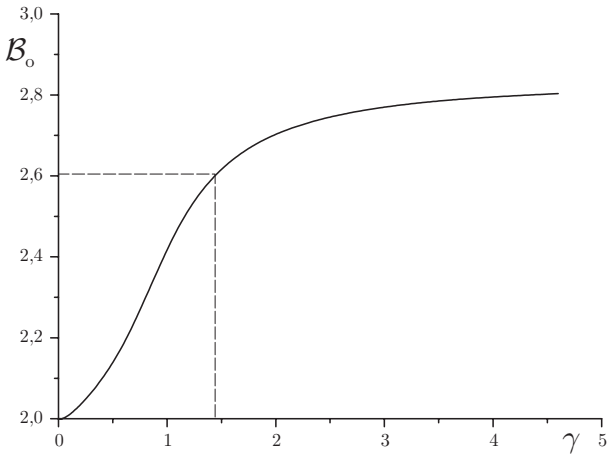

Fig. 2. Maximum value of the Bell signal $\mathcal{B}_o$ [see Eq. (1)] reached for state $|\Psi^+\rangle$ as a function of the NLMS amplitude γ. The '2 photons cat' case, $\gamma = \sqrt{2}$ and $\mathcal{B}_o = 2.61$, is highlighted by the dotted lines.

Wigner function Π. Figure 1a, presents a density plot of $\Pi(\alpha, \beta)$, for $\gamma = 3$, in the plane $\Im(\alpha) = \Im(\beta) = 0$. Three features are conspicuous. The two Gaussian peaks centered at $\alpha = \beta = \pm\gamma$, with a maximum value 0.5, correspond to the two components of the non-local Schrödinger cat state. The central Gaussian peak has a maximum value of +1. It corresponds to an interference feature, revealing the quantum superposition coherence. It is interesting to compare Figures 1a and 1b, which presents the scaled Wigner function for a statistical mixture of $|\gamma, \gamma\rangle$ and $|-\gamma, -\gamma\rangle$ in the same plane. The two components are still present, with the same maximum value 0.5, but the central feature has disappeared.

Since the scaled Wigner function is always positive in this plane, it is clear that the maximum $\mathcal{B}$ value obtained for four real sampling amplitudes is 2, reached when the sampling points are all at the origin. The same value is obtained when both cavities are in the vacuum state. The scaled Wigner function of the vacuum has a single Gaussian peak (maximum value 1) centered at the origin. Note also that the optimum $\mathcal{B}$ value for a statistical mixture [Fig. 1b] is 1. It is obtained with the four sampling points sitting on one of the Gaussian components ($\alpha = \beta = \gamma$ or $\alpha = \beta = -\gamma$), with $\Pi = 0.5$ for all four points.

Violations of the Bell inequality (1) can be found for imaginary sampling amplitudes. Figure 1c presents the scaled Wigner function for imaginary α and β values. The only feature is centered around the origin and is thus linked to the state coherence. It disappears altogether for a statistical mixture of states. This feature is a Gaussian envelope, modulated with interference fringes. The fringes spacing is inversely proportional to the NLMS amplitude γ. For large γ values, the fringes span the entire allowed range for Π, between -1 and $+1$. Choosing sampling points with imaginary amplitudes makes it possible thus to overcome the classical limit in an optimal way.

Figure 1d presents a zoom on this interference feature near the origin. The four sampling points should be on the vertices of a rectangle, with sides parallel to the axes. The ideal situation corresponds to the three points (α', β'), (α, β') and (α', β) close to the maximum of the central positive fringe (which has the maximal contrast), the last point (α, β) being close the minimum of a nearby negative fringe. Moreover, the choice of the points should reflect the obvious symmetries of the fringe pattern (reflection symmetry with respect to the lines $\alpha \pm \beta = 0$).

It is thus natural to choose the four points as the corners of a square, with $\alpha' = \beta'$ and $\alpha = \beta$. The optimal positions are obtained with a numerical optimization on the two remaining parameters, $\Im(\alpha)$ and $\Im(\alpha')$. For $\gamma = 3$, the optimum corresponds to $\alpha' = \beta' = -0.035\,i$ and $\alpha = \beta = 0.095\,i$. The corresponding sampling amplitudes are represented as square dots in Figure 1d. We obtain $\Pi(\alpha', \beta') = 0.664$, $\Pi(\alpha, \beta') = \Pi(\alpha', \beta) = 0.737$ and $\Pi(\alpha, \beta) = -0.63$, corresponding to $\mathcal{B} = 2.77$. Of course, sampling points with opposite amplitudes provide the same $\mathcal{B}$ value. Note that reference [12] examines the violation for the NLMS $|\Phi^-\rangle$. Its scaled Wigner function is very similar (besides a sign change in the interference pattern). The points of optimal violation are thus also in the imaginary plane, contrary to the conclusions of [12].

Figure 2 presents the optimal $\mathcal{B}$ value, $\mathcal{B}_o$, as a function of γ. The Bell inequality (1) is maximally violated ($\mathcal{B}_o = 2\sqrt{2}$) for $\gamma \to \infty$. The optimal sampling points

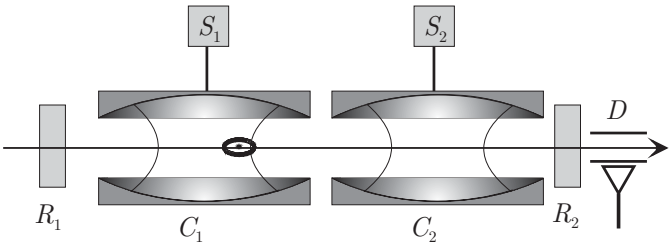

Fig. 3. Proposed experimental set-up. A single circular Rydberg atom crosses successively the two superconducting cavities containing a mesoscopic coherent field. The dispersive atom-cavity interaction creates the NLMS state $|\Psi^+\rangle$. The parity correlations between the two fields is later probed by a second atom.

correspond to the disposition of Figure 1d, with sampling amplitudes going to zero as $1/\gamma$. The largest amplitude NLMS are very sensitive to decoherence processes. A compromise between the amplitude of the inequality violation and the sensitivity to decoherence should thus be reached. A reasonable one corresponds to $\gamma = \sqrt{2}$ ('2 photons cat', dotted lines in Fig. 2). We have then $\mathcal{B}_o = 2.61$ for $\alpha = \beta = 0.175\,i$, $\alpha' = \beta' = -0.05\,i$. Bell's inequality violations are thus expected for relatively small values of γ and small displacements in phase space. This is encouraging for a CQED implementation.

Note that another Bell-type inequality is derived in [11] for the two-mode Q function. It is not adapted, however, to mesoscopic fields situation. The fringes near the origin revealing the non-classical features of a single mode Schrödinger cat state are exponentially suppressed in the Q representation when the amplitude of the cat increases. The same feature is observed with the NLMS studied here. No violations of this Q-function inequality can be observed for $\gamma \geq 1$.

3 Generating NLMS and measuring the Wigner function in CQED

The parity-entangled state $|\Psi^+\rangle$ can be generated in the CQED context with circular Rydberg atoms interacting with two superconducting niobium high-Q microwave cavities [19]. The apparatus is a simple extension of the present one-cavity set-up, described in details in [9]. It is sketched in Figure 3. Rubidium atoms in an atomic beam, velocity-selected by Doppler-resolved optical pumping, are promoted at a well defined time in the long-lived circular Rydberg level e with principal quantum number 51. The average number of atoms per sample is much lower than one, ensuring that no events are recorded with two atoms in the same sample. The atom first interacts, in zone R_1, with a classical microwave field, resonant on the transition to the lower circular level g (principal quantum number 50; $e \rightarrow g$ transition frequency 51.1 GHz). This interaction performs a $\pi/2$ pulse and prepares the atom in state $(|e\rangle + |g\rangle)/\sqrt{2}$.

The atom then crosses the two superconducting cavities C_1 and C_2, both initially prepared in the coherent state $|\lambda\rangle$ by the classical sources S_1 and S_2. The atom interacts dispersively with the cavities, with an atom-field detuning $\delta/2\pi$ of the order of a hundred kHz. The non-resonant atom does not exchange energy with the cavity fields. However, its effective index of refraction transiently modifies the cavity frequency [9]. The classical phase of the coherent amplitude in the cavity is thus modified at the end of the atom-cavity interaction. This phase shift takes opposite values for an atom in e or g. The transformations performed by this interaction are $|e\rangle|\lambda\rangle \rightarrow e^{i\Phi}|e\rangle|\lambda e^{i\Phi}\rangle$ and $|g\rangle|\lambda\rangle \rightarrow |g\rangle|\lambda e^{-i\Phi}\rangle$ where $\Phi = \Omega_0^2 t_i/4\delta$. The 'vacuum Rabi frequency' Ω_0 characterizes the atom-field coupling. It is the frequency of the resonant energy exchange between an excited atom and an empty mode. The effective interaction time t_i takes into account the mode geometry crossed by the atom.

We focus here on the case $\Phi = \pi/2$, reached in realistic experimental conditions, as shown below. The atom-cavities state after the crossing of C_1 and C_2 is thus $(-|e,\gamma,\gamma\rangle + |g,-\gamma,-\gamma\rangle)/\sqrt{2}$, with $\gamma = i\lambda$. The atom then undergoes in zone R_2 a second $\pi/2$ classical pulse resonant on the $e \rightarrow g$ transition and performing the state transformations $|e\rangle \rightarrow (-|e\rangle + |g\rangle)/\sqrt{2}$ and $|g\rangle \rightarrow (|e\rangle + |g\rangle)/\sqrt{2}$. The global state is thus now:

$$|\phi\rangle = \frac{1}{2}\Big[\,|e\rangle\,(|\gamma,\gamma\rangle + |-\gamma,-\gamma\rangle) - |g\rangle\,(|\gamma,\gamma\rangle - |-\gamma,-\gamma\rangle)\Big]. \quad (6)$$

The atom is then detected in the state-selective field ionization counter D. A detection in state e projects the two-cavity system on the NLMS $|\Psi^+\rangle$. We discard, for the present discussion, the events where the atom is finally detected in g, preparing the two-cavity state $|\Phi^-\rangle$.

Note that this procedure could be easily generalized to generate more complex superpositions of coherent states. The non-locality tests proposed in [17], for instance, require entangled two-mode fields made up of four coherent amplitudes in phase space. Such states can be generated by the dispersive interactions of two atoms with the two cavity modes, combined with proper displacements of the cavity fields, realized with the sources S_1 and S_2.

In an ideal non-locality test, the two cavity fields should be separately probed and the Bell signal inferred from the compilation of these separate measurements. The expectation value of the two-mode parity operator can be straightforwardly obtained from a separate measurement of the two cavities Wigner functions, following the method introduced in [14]. It is also possible to infer, from the quantum Rabi oscillation of atoms interacting resonantly with the modes, the photon number distribution in each mode after the translations [20] and hence the parity information [21].

We consider here a much simpler scheme, where the two-mode scaled Wigner function Π is measured by a single atom A_2 crossing the two cavities after A_1. The observation of a Bell inequality violation in these conditions might not rule out without ambiguity 'hidden variables' theories, since the same 'detector' interacts successively

with the two parts of the non-local state. The main goal of these studies is, however, to illustrate the non-local features of quantum mechanics in a new mesoscopic situation and to investigate the Bell signal decoherence properties. The use of a single detector atom makes it simpler to achieve this goal.

The measurement procedure performed by A_2, derived from [14,22], amounts to a measurement of the joint parity operator in the displaced cavity fields [see Eq. (2)]. We first inject with S_1 and S_2 adjustable coherent amplitudes $-\alpha$ and $-\beta$ in C_1 and C_2 respectively. Atom A_2 undergoes the same transformations as A_1 in R_1, C_1, C_2 and R_2. It was shown in [14] that the difference of the probabilities for detecting A_2 in $|e\rangle$ (P_e) and $|g\rangle$ (P_g) provides a direct measurement of the scaled Wigner function when the atom interacts dispersively with a single displaced mode. This result has been generalized to a three-mode case in [22]. It obviously applies also to the two-mode case studied here. More specifically:

$$\Delta P = P_e - P_g = \Pi(\alpha, \beta). \tag{7}$$

In order to test the BW inequality, one has to measure Π at the four optimal sampling points in the two-mode phase space. The measurement of each of these points is performed by accumulating many individual runs of the experiment, that are averaged to obtain the probability difference ΔP.

In any EPR experiment, the observed quantum correlations and the violation of Bell inequalities do not depend upon the timing of the detection events. We have here a similar freedom. The only requirement on the experimental timing is that, for each cavity, the coherent field injection used for the measurement of Π should be performed *after* the interaction with the generating atom A_1 and *before* the interaction with the probe atom A_2. We have implicitly described above a situation where A_2 is sent in the apparatus after A_1 has been detected. The same results would be obtained with a much tighter timing, where A_2 enters C_1 even before A_1 has entered C_2. The minimum time interval between the two atoms thus corresponds roughly to the effective interaction time t_i. This feature has important consequences when it comes to the study of the decoherence of the non-locality signal.

4 Realistic simulation of a feasible experiment

We have discussed so far the principle of an ideal experiment. In an actual realization, many imperfections conspire to reduce the Bell inequality violation, or even to cancel it. It is thus important, in order to assess the interest of the proposed experiment, to perform detailed numerical simulations of the whole set-up, taking into account all known and unavoidable causes of imperfections.

Two main effects are to be taken into account. First, the dispersive atom-cavity interaction results in the simple cavity-field phase-shift effect described above in the perturbative regime, corresponding to an atom-cavity detuning δ much larger than the atom-cavity coupling Ω_0.

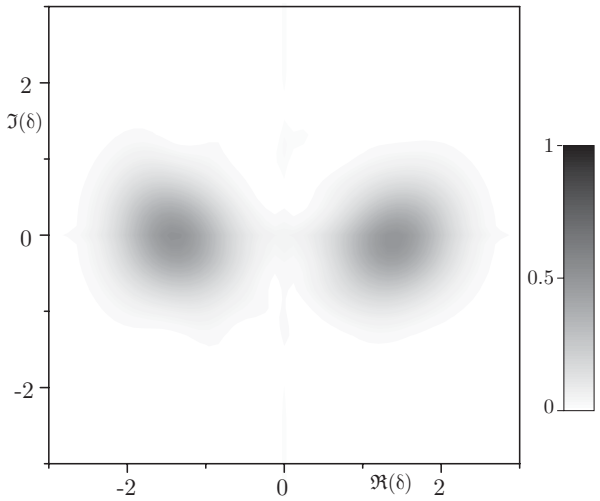

Fig. 4. Scaled Wigner function of cavity C_1, $\Pi_1(\delta)$, after interaction of A_1 with C_1 and C_2, when tracing the global state over C_2 and A_1. This function results from a numerical integration of the exact atom-cavity Hamiltonian. The slight deformation of the coherent components centered at $\pm\sqrt{2}$ is clearly apparent. White corresponds to zero and black to one.

The $\Phi = \pi/2$ condition requires values of δ which are not much bigger than Ω_0. The Wigner function of the resulting NLMS is thus distorted with respect to the ideal shape discussed above. This distortion changes slightly the optimal sampling values α, α', β and β' and affects the maximum value of $\mathcal{B}$.

We thus proceed to a numerical integration of the exact atom-cavity interaction Hamiltonian. The atom-field coupling is chosen to be $\Omega_0/2\pi = 49$ kHz, corresponding to the measured value in the present one-cavity set-up [9]. The coherent field phase shift Φ being proportional to the interaction time t_i, we consider in our simulation the smallest atomic velocity compatible with the actual velocity selection scheme. The velocity of both atoms is thus chosen to be $v = 100$ m/s. The confocal microwave Fabry Perot cavities sustain Gaussian field modes with a waist $w = 6$ mm. The effective interaction time is thus $t_i = \sqrt{\pi} w/(\sqrt{2})v = 75$ μs. The $\Phi = \pi/2$ condition is then met for an atom-field detuning $\delta/2\pi = 160$ kHz.

We first compute the joint scaled Wigner function at the end of the A_1-cavities interaction, for an amplitude $\gamma = \sqrt{2}$. We plot in Figure 4 the scaled Wigner function $\Pi_1(\delta)$ of the field left in C_1 when tracing the global two-cavity state over C_2 and over the atomic state (the cut in the real plane of the global scaled Wigner function Π is not adapted for this discussion, since, for a small γ value, the three features of Figure 1a overlap, making shape distortions less conspicuous). The trace operation leaves in C_1 an incoherent mixture of two phase components, clearly apparent in Figure 4. Note the slight distortion of these components with respect to the ideal Gaussian shape. An identical picture is obtained for the Wigner function of C_2 when tracing over C_1.

We then numerically simulate the measurement of the joint Wigner function by cavity displacements and interaction with the second atom A_2, using the same parameters. We optimize the Bell inequality violations by choosing the displacement amplitudes $\alpha = \beta = 0.27\,i, \alpha' = \beta' = 0.04\,i$. Note that they are noticeably different from the values used in the ideal case. The interference features near the origin, and hence these sampling values, are very sensitive to the precise shape of the scaled Wigner function. We obtain then $\mathcal{B}_o = 2.48$, instead of 2.61 in the ideal case, a value still in the quantum realm. The slight distortion of the Wigner function due to the finite atom-cavity detuning value does not prohibitively affect the observable violation of the BW inequality.

The second, much more important effect to be taken into account is cavity relaxation. It results into a diffusion process for the Wigner function in phase space. This diffusion washes out rapidly the interference fringes at the origin, which are a signature of the non-classical and nonlocal features of the NLMS. The optimal $\mathcal{B}$ value is thus expected to decrease rapidly versus time in a cavity with a finite quality factor Q.

We have taken into account relaxation of both cavities in our numerical simulations. We integrate the full density matrix evolution. We use the same parameters as above, and an atomic velocity of 100 m/s. Atom A_2 is sent through C_1 a delay T after A_1. As already mentioned, we have a complete freedom on the experimental timing, provided A_2 enters C_1 after the displacement operation, which is performed after the exit of A_1. We allow thus the minimum value of T to be 240 μs. The distance between A_1 and A_2 is then 24 mm, much larger than the cavity modes extension ($2w = 12$ mm). The interactions of the two atoms with both cavity modes are thus independent. Note that the displacement operation is basically instantaneous on the experimental time scale.

Once A_2 exits C_1, all the relevant quantum information is stored in the atomic states, which are very long-lived. Further decoherence processes in C_1 during the time of flight T_f of the two atoms between C_1 and C_2 thus do not play any role in the observed $\mathcal{B}_o$ value. This is particularly important, since the minimal realistic distance between the cavity axes is of the order of 10 cm (cavity mirror diameter 5 cm), corresponding to $T_f \approx 1$ ms. We assume that the timing of the events in C_2 is exactly the same as in C_1, merely translated by the time of flight T_f. Figure 5 summarizes the global timing.

Figure 6 presents the optimal $\mathcal{B}$ values at short times versus the delay T for two cavities with $Q = 10^{10}$, corresponding to a field energy lifetime $T_c = 30$ ms (squares), and $Q = 10^{11}$, corresponding to $T_c = 300$ ms (disks). For each delay, we perform an optimization of the sampling amplitudes $\Im(\alpha')$ and $\Im(\alpha)$. At short times, these amplitudes are not affected by relaxation. The contrast of the fringes in the imaginary plane [see Fig. 1d], and hence the $\mathcal{B}_o$ value, drop rapidly due to the diffusion process, but the position of the fringes extrema is nearly constant. The lines in Figure 6 are exponential fits on the initial decay. The corresponding time constants, 4.3 and 40 ms, give an estimate of the decoherence time scale, of the order of $T_c/D^2 = T_c/8$, where $D = 2\sqrt{2}$ is the 'distance' between the two cat components.

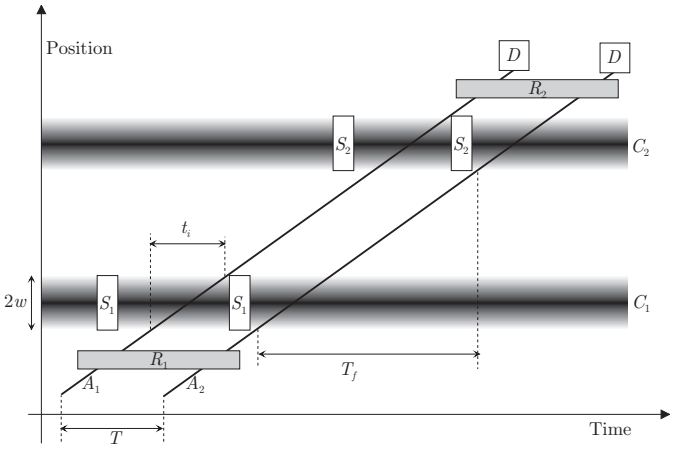

Fig. 5. Timing of the proposed experiment. The time is along the horizontal axis, the position along the vertical one. The two cavity modes are represented by the shaded areas. The two atoms correspond to the parallel oblique lines. The field injection events are represented by the white rectangles on the cavity modes. The resonant mixing pulses R_1 and R_2 are represented by the horizontal gray rectangles.

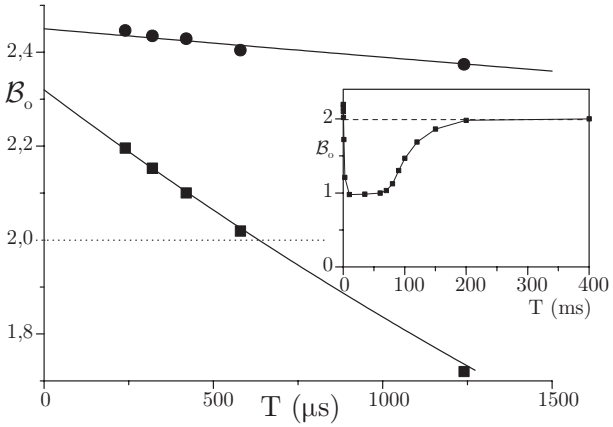

Fig. 6. Results of the complete numerical simulation of the proposed experiment. Squares: computed values of the optimal Bell signal $\mathcal{B}_o$ for an initial two-photon field as a function of the delay T between the two atoms for $T_c = 30$ ms ($Q = 10^{10}$). Disks: $\mathcal{B}_o(T)$ for $T_c = 300$ ms ($Q = 10^{11}$). Lines are exponential fits with decay time constants of 4.3 and 40 ms. Inset: long-time behavior of $\mathcal{B}_o(T)$ for $T_c = 30$ ms. The line connecting the computed points has been added for visual convenience.

This rapid decay stops when the $\mathcal{B}_o$ value reaches 1, the value for a statistical mixture. This occurs, for the shortest cavity damping time, around $T = 10$ ms. The optimal sampling points are, from then on, in the real plane, sitting on the top of one of the components of the statistical mixture: $\alpha' = \beta' = \alpha = \beta$, all of them being real. These sampling values follow the slow decay of the amplitude of the two mixed states.

At much longer times, of the order of a few cavity damping times, the amplitudes of the fields in both cavities finally decay to zero. The optimal $\mathcal{B}$ value returns thus slowly to 2. The long time behaviour of $\mathcal{B}_o$ is plotted in the inset of Figure 6 for $Q = 10^{10}$. The fast drop of the initial violation is almost instantaneous on this time scale. A plateau near $\mathcal{B}_o = 1$ is observed between 10 and 80 ms, followed by the slow return to the vacuum value $\mathcal{B}_o = 2$.

Figure 6 thus shows that significant violations of Bell inequalities could be observed with $\gamma = 2$ on a significant time delay span. For smaller cat amplitudes, the decoherence time scale is longer. The decoherence-free optimal value of $\mathcal{B}$ is nevertheless smaller and significantly larger violations of Bell inequalities are not expected. The fast decrease of the decoherence time scale with γ, on the other hand, precludes the use of much larger cat amplitudes. The two-photon cat considered here appears as a good compromise for Q values which are not out of reach for superconducting cavities [23].

5 Conclusions

We have shown that cavity QED techniques with circular Rydberg atoms and superconducting cavities are well suited to the production of non-local mesoscopic state superpositions by a single atom interacting successively with two cavity modes. The violation of a Bell-type inequality, adapted to this continuous variable situation, reveals the non-local nature of this cat. A readout atom is used to perform the corresponding measurements.

We have carefully analyzed the expected experimental imperfections. A realistic simulation of the atom-cavity interaction exhibits a slight distortion of the non-local state, as compared to the ideal situation. A clear violation of the Bell inequality is nevertheless still observable. Cavity relaxation is a more serious obstacle, since state preparation and read out require a time interval not negligible at the scale of the decoherence time. We have shown that Bell inequalities violations could nevertheless be observed with cavity damping times in the 30 ms range. This is larger that the present performances of open Fabry Perot cavities ($T_c = 1$ ms), but well within reach of superconducting cavities technologies. There is thus a good hope to observe quantum non-locality on mesoscopic states with a two-cavity Rydberg-atom set-up, presently under construction in our laboratory.

Laboratoire Kastler Brossel, ENS and Université Pierre et Marie Curie, is associated with CNRS (UMR 8552). This work is supported by the JST agency (Quantum entanglement ICORP project) and by European Community (QUEST, CONQUEST, QUBITS and QUGATES programs).

References

1. A. Einstein, B. Podolski, N. Rosen, Phys. Rev. **47**, 777 (1935)
2. J.S. Bell, Physics **1**, 195 (1964)
3. J.F. Clauser, M.A. Horne, A. Shimony, R.A. Holt, Phys. Rev. Lett. **23**, 880 (1969)
4. J.F. Clauser, Phys. Rev. Lett. **36**, 1223 (1976); A. Aspect, P. Grangier, G. Roger, Phys. Rev. Lett. **47**, 460 (1981); G. Weihs et al., Phys. Rev. Lett. **81**, 5039 (1998); M.A. Rowe et al., Nature **409**, 791 (2001); R.T. Thew et al., Phys. Rev. A **66**, 062304 (2002)
5. D. Giulini, E. Joos, C. Kiefer, J. Kupsch, I.-O. Stamatescu, H.D. Zeh, *Decoherence and the Appearance of a Classical World in Quantum Theory* (Springer-Verlag, Berlin, 1996) and references therein
6. F. Grosshans, P. Grangier, Phys. Rev. Lett. **88**, 057902 (2002); F. Grosshans, G. Van Assche, J. Wenger, R. Brouri, N.J. Cerf, P. Grangier, Nature **421**, 238 (2003)
7. C.H. Bennett, G. Brassard, *Proc. of the Intl. Conf. Computer Systems and Signal Processing*, Bangalore, India, p. 175; C.H. Bennett, G. Brassard, D. Mermin, Phys. Rev. Lett. **68**, 557 (1992)
8. D. Wilson, H. Jeong, M.S. Kim, J. Mod. Opt. **49**, 851 (2002)
9. J.M. Raimond, M. Brune, S. Haroche, Rev. Mod. Phys. **73**, 565 (2001)
10. M. Brune et al., Phys. Rev. Lett. **77**, 4887 (1996)
11. K. Banaszek, K. Wódkiewicz, Phys. Rev. Lett. **82**, 2009 (1999)
12. H. Jeong, W. Son, M.S. Kim, D. Ahn, C. Brukner, Phys. Rev. A **67**, 012106 (2003)
13. E. Wigner, Phys. Rev. **40**, 749 (1932); for a review, see M. Hillery et al., Phys. Rep. **106**, 121 (1984)
14. L.G. Lutterbach, L. Davidovich, Phys. Rev. Lett. **78**, 2547 (1997)
15. P. Bertet et al., Phys. Rev. Lett. **89**, 200402 (2002)
16. K.E. Cahill, R.J. Glauber, Phys. Rev. **177**, 1857 (1969); Phys. Rev. **177**, 1882 (1969)
17. J. Wenger, M. Hafezi, F. Grosshans, R. Tualle-Brouri, P. Grangier, Phys. Rev. A **67**, 012105 (2003)
18. R. Garcia-Patron-Sanchez et al., preprint `arXiv:Quant-Phys/0403191`
19. L. Davidovich et al., Phys. Rev. A **53**, 1295 (1996)
20. M. Brune et al., Phys. Rev. Lett. **76**, 1800 (1996)
21. D. Leibfried et al., Phys. Rev. Lett. **77**, 4281 (1996)
22. M. França Santos, L.G. Lutterbach, L. Davidovich, J. Opt. B: Quant. Semiclass. Opt. **3**, S55 (2001)
23. M. Weidinger et al., Phys. Rev. Lett. **82**, 3795 (1999)